Pseudogaps in strongly correlated metals: A generalized dynamical mean-field theory approach

M. V. Sadovskii,[1] I. A. Nekrasov,[1,2] E. Z. Kuchinskii,[1] Th. Pruschke,[3] and V. I. Anisimov[2]

[1]*Institute for Electrophysics, Russian Academy of Sciences, Ekaterinburg, 620016, Russia*
[2]*Institute for Metal Physics, Russian Academy of Sciences, Ekaterinburg, 620219, Russia*
[3]*Institut für Theoretische Physik, Universität Göttingen, Germany*

We generalize the dynamical-mean field (DMFT) approximation by including into the DMFT equations some length scale ξ via a momentum dependent external self-energy $\Sigma_{\mathbf{k}}$. This external self-energy describes nonlocal dynamical correlations induced by the short-ranged collective spin density wave–like antiferromagnetic spin (or the charge density wave–like charge) fluctuations. At high enough temperatures these fluctuations can be viewed as a quenched Gaussian random field with a finite correlation length. This generalized DMFT+$\Sigma_{\mathbf{k}}$ approach is used for the numerical solution of the weakly doped one-band Hubbard model with repulsive Coulomb interaction on a square lattice with the nearest and the next nearest neighbor hopping. The effective single impurity problem in this generalized DMFT+$\Sigma_{\mathbf{k}}$ is solved by the numerical renormalization group. Both types of the strongly correlated metals, namely: (i) The doped Mott insulator and (ii) the case of the bandwidth $W \lesssim U$ (U—value of the local Coulomb interaction) are considered. The densities of states, the spectral functions, and the angle resolved photoemission spectra calculated within the DMFT+$\Sigma_{\mathbf{k}}$ show a pseudogap formation near the Fermi level of the quasiparticle band.

I. INTRODUCTION

Among the numerous anomalies of the normal phase of high-temperature superconductors the observation of a pseudogap in the electronic spectrum of underdoped copper oxides[1,2] is especially interesting. Despite continuing discussions on the nature of the pseudogap, the preferable scenario for its formation is most likely based on the model of strong scattering of the charge carriers by a short-ranged antiferromagnetic (AFM) or spin density wave (SDW) spin fluctuations.[2,3] In a momentum representation, this scattering transfers momenta of the order of $\mathbf{Q}=(\pi/a, \pi/a)$ (a—lattice constant of a two-dimensional lattice). This leads to the formation of structures in the one-particle spectrum, which are precursors of the changes in the spectra due to the long-range AFM order (period doubling). As a result, we obtain non-Fermi-liquidlike behavior (dielectrization) of the spectral density in the vicinity of the so called hot spots on the Fermi surface, appearing at intersections of the Fermi surface with an antiferromagnetic Brillouin zone boundary (Umklapp surface).[2]

Within this spin-fluctuation scenario, a simplified model of the pseudogap state was studied[2,4,5] under the assumption that the scattering by dynamic spin fluctuations can be reduced for high enough temperatures to a static Gaussian random field (quenched disorder) of pseudogap fluctuations. These fluctuations are defined by a characteristic scattering vector from the vicinity of $\mathbf{Q}$, with a width determined by the inverse correlation length of a short-range order $\kappa=\xi^{-1}$, and by an appropriate energy scale Δ (typically of the order of the crossover temperature T^* to the pseudogap state[2]).

Undoped cuprates are antiferromagnetic Mott insulators with $U \gg W$ (U—value of the local Coulomb interaction, W—bandwidth of noninteracting band), so that correlation effects are very important. It is thus clear that the electronic properties of underdoped (and probably also optimally doped) cuprates are governed by strong electronic correlations also, so that these systems are typical strongly correlated metals. Two types of correlated metals can be distinguished: (i) the doped Mott insulator and (ii) the bandwidth controlled correlated metal $W \approx U$. Both types will be considered in this paper.

A state of the art tool to describe such correlated systems is the dynamical mean-field theory (DMFT).[6–10] The characteristic features of correlated systems within the DMFT are the formation of incoherent structures, the so-called Hubbard bands, split by the Coulomb interaction U, and a quasiparticle (conduction) band near the Fermi level dynamically generated by the local correlations.[6–10]

Unfortunately, the DMFT is not useful to the study of the antiferromagnetic scenario of the pseudogap formation in strongly correlated metals. This is due to the basic approximation of the DMFT, which amounts to the complete neglect of nonlocal dynamical correlation effects.

Besides the extended DMFT,[11] which locally includes a coupling to nonlocal dynamical fluctuations, a straightforward way to extend the DMFT are the so-called cluster mean-field theories.[12] Two variants of this approach are the dynamical cluster approximation (DCA) (Ref. 12) and the cellular DMFT (CDMFT).[13] In particular, the DCA has been applied to study the low-energy properties of the Hubbard model, systematically including short- to medium-ranged nonlocal correlations. Both improve on the cluster perturbation theory (CPT),[14,15] an attempt to use finite-size calculations to obtain approximate results for the thermodynamic limit.

However, these approaches have certain drawbacks from both the technical and the interpretation points of view. First, the effective quantum single impurity problem becomes rather complex. Thus, most computational methods available for the DMFT can be applied for the smallest clusters only,[12,16,17] i.e., include nearest-neighbor fluctuations only. For medium- to long-ranged correlations one is currently re-

stricted to the Quantum Monte-Carlo.[18,19] Since for cluster problems again a sign problem arises, one is restricted to relatively small values of the local Coulomb interaction and high temperatures. Second, the interpretation of electronic structures found has to be based on a reliable input from other, typically approximate, complementary techniques.

The aim of the present paper is to propose such an approach, which on the one hand retains the single-impurity description of the DMFT, viz a proper account for *local* correlations and the possibility of using very efficient impurity solvers like NRG;[20,21] on the other hand, we include nonlocal correlations on a nonperturbative model basis, which allows one to control characteristic scales and also types of nonlocal fluctuations. This latter point allows for a systematical study of the influence of a nonlocal fluctuation on the electronic properties and in particular provide valuable hints on the physical origin and the possible interpretation of results found in, e.g., more refined theoretical approaches.

The paper is organized as follows: In Sec. II we present a derivation of the self-consistent generalization we call DMFT+$\Sigma_{\mathbf{k}}$ which includes short-ranged dynamical correlations to some extent. Section III describes the construction of the **k**-dependent self-energy, and some computational details are presented in Sec. IV A. Results and discussion are given in the Sec. IV. Then the paper is ended with a summary (Sec. V) together with an overview of related recent approaches and results on a pseudogap issue.

II. INTRODUCING LENGTH SCALE INTO DMFT: DMFT+$\Sigma_{\mathbf{k}}$ APPROACH

The basic shortcoming of the traditional DMFT approach[6–10] is the neglect of the momentum dependence of the electron self-energy. This approximation, in principle, allows for an exact solution of the correlated electron systems fully preserving the local part of the dynamics introduced by electronic correlations. To include nonlocal effects, while remaining within the usual single impurity analogy, we propose the following procedure. To be definite, let us consider a standard one-band Hubbard model from now on. The extension to multi-orbital or multi-band models is straightforward. The major assumption of our approach is that the lattice and Matsubara time Fourier transformed of the single-particle Green function can be written as:

$$G_{\mathbf{k}}(i\omega) = \frac{1}{i\omega + \mu - \varepsilon(\mathbf{k}) - \Sigma(i\omega) - \Sigma_{\mathbf{k}}(i\omega)}, \quad \omega = \pi T(2n+1),$$

(1)

where $\Sigma(i\omega)$ is the *local* contribution to the self-energy, surviving in the DMFT, while $\Sigma_{\mathbf{k}}(i\omega)$ is a momentum dependent part. We suppose that this last contribution is due to either electron interactions with some additional collective modes or order parameter fluctuations, or may be due to a similar nonlocal contribution within the Hubbard model itself.

To avoid possible confusion, we must stress that $\Sigma_{\mathbf{k}}(i\omega)$ can, in principle, also contain local (momentum independent) contributions, which obviously *vanish* in the limit of an infinite dimensionality $d \to \infty$ and are not taken into account

within the DMFT. Due to this fact there is no double counting of diagrams within our approach to the Hubbard model. This question does not arise at all if we consider $\Sigma_{\mathbf{k}}(i\omega)$ appearing due to some additional interaction. More important is that the assumed additive form of the self-energy $\Sigma(i\omega) + \Sigma_{\mathbf{k}}(i\omega)$ implicitly corresponds to the neglect of possible interference of these local (DMFT) and nonlocal contributions. Furthermore, both contributions to the total self-energy $\Sigma(i\omega) + \Sigma_{\mathbf{k}}(i\omega)$ individually obey causality by construction. Thus, the sum and finally the propagator (1) constructed from it are causal, too.

The self-consistency equations of our generalized DMFT+$\Sigma_{\mathbf{k}}$ approach are formulated as follows.

(1) Start with some initial guess of *local* self-energy $\Sigma(i\omega)$, e.g., $\Sigma(i\omega) = 0$.

(2) Construct $\Sigma_{\mathbf{k}}(i\omega)$ within some (approximate) scheme, taking into account interactions with collective modes or order parameter fluctuations which in general can depend on $\Sigma(i\omega)$ and μ.

(3) Calculate the local Green function

$$G_{ii}(i\omega) = \frac{1}{N} \sum_{\mathbf{k}} \frac{1}{i\omega + \mu - \varepsilon(\mathbf{k}) - \Sigma(i\omega) - \Sigma_{\mathbf{k}}(i\omega)}.$$

(2)

(4) Define the "Weiss field"

$$\mathcal{G}_0^{-1}(i\omega) = \Sigma(i\omega) + G_{ii}^{-1}(i\omega).$$

(3)

(5) Use some "impurity solver" to calculate the single-particle Green function for the effective single Anderson impurity problem, defined by the Grassmanian integral

$$G_d(\tau - \tau') = \frac{1}{Z_{\text{eff}}} \int Dc_{i\sigma}^{\dagger} Dc_{i\sigma}^{\dagger} c_{i\sigma}(\tau) c_{i\sigma}^{\dagger}(\tau') \exp(-S_{\text{eff}})$$ (4)

with the effective action for a fixed site ("single impurity") i

$$S_{\text{eff}} = -\int_0^{\beta} d\tau_1 \int_0^{\beta} d\tau_2 \, c_{i\sigma}(\tau_1) \mathcal{G}_0^{-1}(\tau_1 - \tau_2) c_{i\sigma}^{\dagger}(\tau_2)$$

$$+ \int_0^{\beta} d\tau \, U n_{i\uparrow}(\tau) n_{i\downarrow}(\tau),$$

(5)

$Z_{\text{eff}} = \int Dc_{i\sigma}^{\dagger} Dc_{i\sigma} \exp(-S_{\text{eff}})$, and $\beta = T^{-1}$. This step produces a *new* set of values $G_d^{-1}(i\omega)$.

(6) Define a *new* local self-energy

$$\Sigma(i\omega) = \mathcal{G}_0^{-1}(i\omega) - G_d^{-1}(i\omega).$$

(6)

(7) Using this self-energy as an initial one in step (1), continue the procedure until (and if) convergency is reached to obtain

$$G_{ii}(i\omega) = G_d(i\omega).$$

(7)

Eventually, we get the desired Green function in the form of (1), where $\Sigma(i\omega)$ and $\Sigma_{\mathbf{k}}(i\omega)$ are those appearing at the end of our iteration procedure. A more detailed derivation of this scheme within a diagrammatic approach is given in Appendix A.

III. CONSTRUCTION OF k-DEPENDENT SELF-ENERGY

For the momentum dependent part of the single-particle self-energy we concentrate on the effects of the scattering of electrons from the collective short-range SDW–like antiferromagnetic spin [or charge density wave (CDW)–like charge] fluctuations. To calculate $\Sigma_\mathbf{k}(i\omega)$ for an electron moving in the quenched random field of (static) Gaussian spin (or charge) fluctuations with dominant scattering momentum transfers from the vicinity of some characteristic vector $\mathbf{Q}$ (hot spots model[2]), we use a slightly generalized version of the recursion procedure proposed in Refs. 4, 5, and 22 which takes into account *all* the Feynman diagrams describing the scattering of the electrons by this random field. This becomes possible due to a remarkable property of our simplified version of hot spots model that under certain conditions the contribution of an arbitrary diagram with intersecting interaction lines is actually equal to the contribution of some diagram of the same order without intersections of these lines.[5,22] Thus, in fact, we can limit ourselves to consideration of only diagrams without intersecting interaction lines, taking the contribution of diagrams with intersections into account with the help of additional combinatorial factors, which are attributed to "initial" vertices or just interaction lines.[22] As a result, we obtain the following recursion relation (continuous fraction representation[22]):

$$\Sigma_n(i\omega,\mathbf{k}) = \Delta^2 \frac{s(n)}{i\omega + \mu - \Sigma(i\omega) - \varepsilon_n(\mathbf{k}) + inv_n\kappa - \Sigma_{n+1}(i\omega,\mathbf{k})}.$$

$$(8)$$

The term $\Sigma_n(i\omega,\mathbf{k})$ of recurring sequence contains all contributions of diagrams with the number of interaction lines $\geq n$. Then

$$\Sigma_\mathbf{k}(i\omega) = \Sigma_{n=1}(i\omega,\mathbf{k}) \qquad (9)$$

is actually the sum of all diagrammatic contributions. Since the convergence of this recursion procedure for $\Sigma_n(i\omega,\mathbf{k})$ is rather fast, one can set contributions for large enough n equal to zero and doing recursion backwards to $n=1$ to get the desired physical self-energy.[5]

The quantity Δ characterizes the energy scale and $\kappa = \xi^{-1}$ is the inverse correlation length of the short-range SDW (CDW) fluctuations, $\varepsilon_n(\mathbf{k}) = \varepsilon(\mathbf{k}+\mathbf{Q})$ and $v_n = |v^x_{\mathbf{k}+\mathbf{Q}}| + |v^y_{\mathbf{k}+\mathbf{Q}}|$ for odd n while $\varepsilon_n(\mathbf{k}) = \varepsilon(\mathbf{k})$ and $v_n = |v^x_\mathbf{k}| + |v^y_\mathbf{k}|$ for even n. The velocity projections $v^x_\mathbf{k}$ and $v^y_\mathbf{k}$ are determined by usual momentum derivatives of the "bare" electronic energy dispersion $\varepsilon(\mathbf{k})$. Finally, $s(n)$ represents a combinatorial factor with

$$s(n) = n \qquad (10)$$

for the case of commensurate charge (CDW-type) fluctuations with $\mathbf{Q} = (\pi/a, \pi/a)$.[22] For the incommensurate CDW fluctuations[22] (when $\mathbf{Q}$ is not locked to the period of the reciprocal lattice) one finds

$$s(n) = \begin{cases} \dfrac{n+1}{2} & \text{for odd } n \\[2mm] \dfrac{n}{2} & \text{for even } n. \end{cases} \qquad (11)$$

If we want to take into account the (Heisenberg) spin structure of interaction with spin fluctuations in nearly antiferromagnetic Fermi-liquid [spin-fermion (SF) model of Ref. 4, SDW-type fluctuations], the combinatorics of the diagrams becomes more complicated. Spin-conserving scattering processes obey commensurate combinatorics, while spin-flip scattering is described by the diagrams of incommensurate type (charged random field in terms of Ref. 4). In this model, the recursion relation for the single-particle Green function is again given by (8), but the combinatorial factor $s(n)$ now acquires the following form:[4]

$$s(n) = \begin{cases} \dfrac{n+2}{3} & \text{for odd } n \\[2mm] \dfrac{n}{3} & \text{for even } n. \end{cases} \qquad (12)$$

Obviously, with this procedure we introduce an important length scale ξ not present in standard DMFT. Physically this scale mimics the effect of short-range (SDW or CDW) correlations within fermionic bath surrounding the effective single Anderson impurity of the DMFT. We expect that such a length scale will lead to a competition between local and nonlocal physics.

An important aspect of the theory is that both parameters Δ and ξ can, in principle, be calculated from the microscopic model at hand. For example, using the two-particle self-consistent approach of Ref. 23 with the approximations introduced in Refs. 4 and 5, one can derive within the standard Hubbard model the following microscopic expression for Δ:

$$\Delta^2 = \frac{1}{4}U^2\frac{\langle n_{i\uparrow}n_{i\downarrow}\rangle}{\langle n_{i\uparrow}\rangle\langle n_{i\downarrow}\rangle}[\langle n_{i\uparrow}\rangle + \langle n_{i\downarrow}\rangle - 2\langle n_{i\uparrow}n_{i\downarrow}\rangle]$$

$$= U^2\frac{\langle n_{i\uparrow}n_{i\downarrow}\rangle}{n^2}\langle (n_{i\uparrow} - n_{i\downarrow})^2\rangle = U^2\frac{\langle n_{i\uparrow}n_{i\downarrow}\rangle}{n^2}\frac{1}{3}\langle \vec{S}_i^2\rangle, \quad (13)$$

where we consider only scattering from antiferromagnetic spin fluctuations. The different local quantities—spin fluctuation $\langle \vec{S}_i^2\rangle$, density n and double occupancy $\langle n_{i\uparrow}n_{i\downarrow}\rangle$—can easily be calculated within the standard DMFT.[9] A detailed derivation of (13) and the computational results for Δ obtained by the DMFT using the quantum Monte-Carlo (QMC) to solve the effective single impurity problem are presented in Appendix B. A corresponding microscopic expression for the correlation length ξ can also be derived within the two-particle self-consistent approach.[23] However, we expect those results for ξ to be less reliable, because this approach is valid only for relatively small (or medium) values of U/t. Thus, in the following, we will consider both Δ and especially ξ as some phenomenological parameters to be determined from the experiments.

IV. RESULTS AND DISCUSSION

A. Computation details

In the following, we want to discuss the results for a standard one-band Hubbard model on a square lattice. With the nearest (t) and next nearest (t') neighbor hopping integrals the dispersion then reads

$$\varepsilon(\mathbf{k}) = -2t(\cos k_x a + \cos k_y a) - 4t' \cos k_x a \cos k_y a, \tag{14}$$

where a is the lattice constant. The correlations are introduced by a repulsive local two-particle interaction U. We choose as an energy scale, the nearest neighbor hopping integral t and as a length scale, the lattice constant a.

For a square lattice the bare bandwidth is $W = 8t$. To study a strongly correlated metallic state obtained as a doped Mott insulator we use $U = 40t$ as a value for the Coulomb interaction and a filling $n = 0.8$ (hole doping). The particular choice of the latter value for U is motivated by two aspects. First, this value of U leads to an insulating DMFT+$\Sigma_\mathbf{k}$, solution at half-filling. Second, the estimations of U for the stoichiometric La$_2$CuO$_4$ (high-T_C prototype compound) based on the constrained LDA (Ref. 24) calculations typically give U of the order of 10 eV,[25] which corresponds to $40t$ with our choice of parameters. The correlated metal in the case of $W \gtrsim U$ is realized via $U = 4t$—a value used in various theoretical papers discussing the pseudogap state—and two fillings: half-filling ($n = 1.0$) and $n = 0.8$ (hole doping). As typical values for Δ we choose $\Delta = t$ and $\Delta = 2t$ (actually as approximate limiting values—see Appendix B) and for the correlation length $\xi = 2a$ and $\xi = 10a$ (motivated mainly by the experimental data for cuprates[2,4]).

The DMFT maps the lattice problem onto an effective, self-consistent single impurity defined by Eqs. (4) and (5). In our work, we employ as "impurity solvers" two reliable numerically exact methods—quantum Monte-Carlo (QMC) (Ref. 18) and the numerical renormalization group (NRG).[20,21] The calculations were done for the case $t' = 0$ and $t'/t = -0.4$ (more or less typical for cuprates) at two different temperatures $T = 0.088t$ and $T = 0.356t$ (for NRG computations).[40] QMC computations of double occupancies as functions of filling were done at temperatures $T = 0.1t$ and $T = 0.4t$.[41]

Below we present results only for most typical dependences and parameters, more data and figures can be found in Ref. 26.

B. Generalized DMFT+$\Sigma_\mathbf{k}$ approach: densities of states

Let us start the discussion of our results obtained within our generalized DMFT+$\Sigma_\mathbf{k}$ approach with the densities of states (DOS) for the case of the small (relative to bandwidth) Coulomb interaction $U = 4t$ with and without pseudogap fluctuations. As already discussed in Sec. I, the characteristic feature of the strongly correlated metallic state is the coexistence of the lower and upper Hubbard bands split by the value of U with a quasiparticle peak at the Fermi level. Since at half-filling the bare DOS of the square lattice has a Van–Hove singularity at the Fermi level ($t' = 0$) or close to it (in
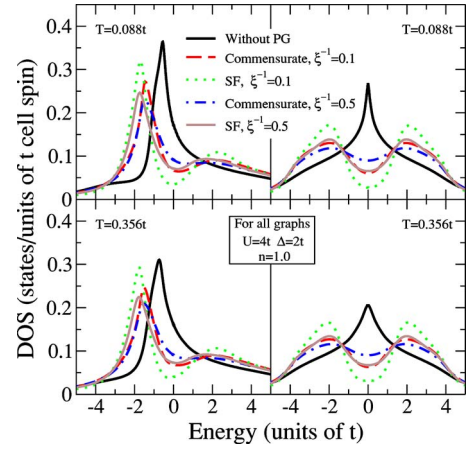

FIG. 1. (Color online) Comparison of DOS obtained from DMFT(NRG)+$\Sigma_\mathbf{k}$ calculations for different combinatorical factors (SF–spin-fermion model, commensurate), inverse correlation lengths (ξ^{-1}) in units of the lattice constant, temperatures (T), and the value of pseudogap potential $\Delta = 2t$. The left column corresponds to $t'/t = -0.4$, the right column to $t' = 0$. In all graphs the Coulomb interaction is $U = 4t$ and $n = 1$. The Fermi level corresponds to zero.

case of $t'/t = -0.4$) one cannot treat a peak on the Fermi level simply as a quasiparticle peak. In fact, there are two contributions to this peak; (i) the quasiparticle peak appearing in a strongly correlated metals due to many-body effects and (ii) the smoothed Van–Hove singularity from the bare DOS.[42] In Figs. 1 and 2 we show the corresponding DMFT (NRG) DOS without pseudogap fluctuations as black lines for both the bare dispersions $t'/t = -0.4$ (left panels) and for the $t' = 0$ (right panels) for two different temperatures $T = 0.356t$ (lower panels) and $T = 0.088t$ (upper panels) with fillings $n = 1.0$ and $n = 0.8$, respectively. The remaining curves in Figs. 1 and 2 represent results for the DOS with nonlocal fluctuations switched on with the fluctuation amplitude $\Delta = 2t$. For all sets of parameters, one can see that the introduction of nonlocal fluctuations into the calculation leads to the formation of pseudogap in the quasiparticle peak.
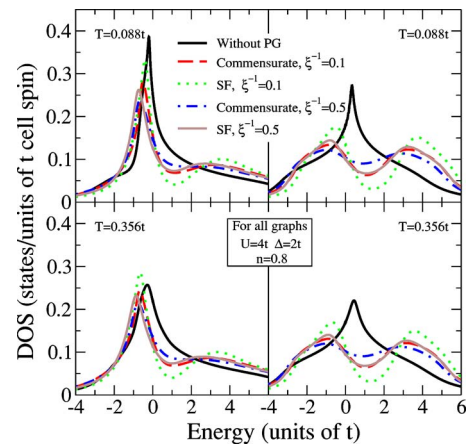

FIG. 2. (Color online) Comparison of DOS obtained from DMFT(NRG)+$\Sigma_\mathbf{k}$ calculations for a filling $n = 0.8$, other parameters as in Fig. 1.
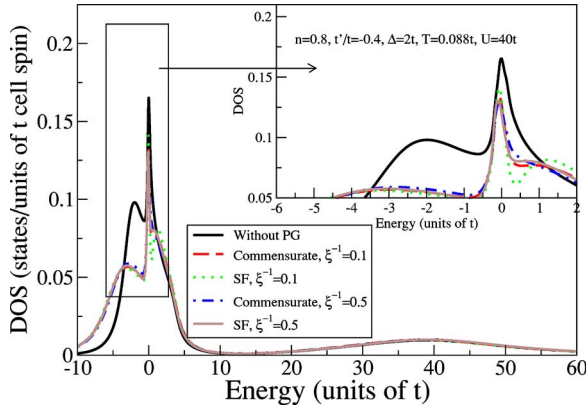
FIG. 3. (Color online) Comparison of DOS obtained from DMFT(NRG)+$\Sigma_{\mathbf{k}}$ calculations for $t'/t=-0.4$, $T=0.088t$, $U=40t$, $\Delta=2t$, and filling $n=0.8$.

The behavior of the pseudogaps in the DOS has some common features. For example, for $t'=0$ at half-filling (Fig. 1, right column) we find that the pseudogap is most pronounced. For $n=0.8$ (Fig. 2, right column) the picture is almost the same but slightly asymmetric. The width of the pseudogap (the distance between the peaks closest to the Fermi level) appears to be of the order of $\sim 2\Delta$ here. Decreasing the value of Δ from $2t$ to t leads to a pseudogap that is correspondingly twice smaller and in addition more shallow (see Ref. 26). When one uses the combinatorial factors corresponding to the spin-fermion model [Eq. (12)], we find that the pseudogap becomes more pronounced than in the case of commensurate charge fluctuations [combinatorial factors of Eq. (11)]. The influence of the correlation length ξ can be seen as expected. Changing from $\xi^{-1}=0.1$ to $\xi^{-1}=0.5$, i.e., decreasing the range of the nonlocal fluctuations, slightly washes out the pseudogap. Also, increasing the temperature from $T=0.088t$ to $T=0.356t$ leads to a general broadening of the structures in the DOS. These observations remain at least qualitatively valid for $t'/t=-0.4$ (Figs. 1 and 2, left columns) with an additional asymmetry due to the next-nearest neighbor hopping. Noteworthy is, however, the fact that for $t'/t=-0.4$ and $\xi^{-1}=0.5$ the pseudogap has almost disappeared for the temperatures studied here. Also a very remarkable point is the similarity of the results obtained with the generalized DMFT+$\Sigma_{\mathbf{k}}$ approach with $U=4t$ (smaller than the bandwidth W) to those obtained earlier without the Hubbard-like Coulomb interactions.[4,5]

Let us now consider the case of a doped Mott insulator. The model parameters are $t'/t=-0.4$ with filling $n=0.8$, but the Coulomb interaction strength is now set to $U=40t$. The characteristic features of the DOS for such a strongly correlated metal are a strong separation of the lower and upper Hubbard bands and a Fermi level crossing by the lower Hubbard band (for the non-half-filled case). Without nonlocal fluctuations the quasiparticle peak is again formed at the Fermi level; but now the upper Hubbard band is far to the right and does not touch the quasiparticle peak (as it was for the case of small Coulomb interactions). DOS without nonlocal fluctuations are again presented as black lines in Fig. 3. The results for the case $t'=0$ are presented elsewhere.[26]

With rather strong nonlocal fluctuations $\Delta=2t$, a pseudogap appears in the middle of the quasiparticle peak. In
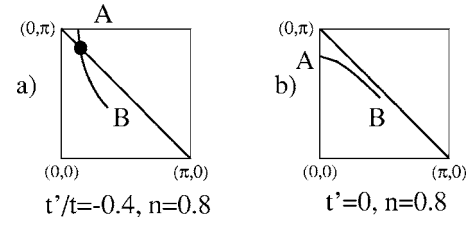

FIG. 4. One-eighth of the bare Fermi surfaces for the occupancy $n=0.8$ and different combinations (t,t') used for the calculation of spectral functions $A(\mathbf{k},\omega)$. The diagonal line corresponds to the Umklapp surface. The full circle marks the so-called hot spot.

addition, we observe that the lower Hubbard band is slightly broadened by fluctuation effects. Qualitative behavior of the pseudogap anomalies is again similar to those described above for the case of $U=4t$, e.g., a decrease of ξ makes the pseudogap less pronounced, reducing Δ from $\Delta=2t$ to $\Delta=t$ narrows of the pseudogap and also makes it more shallow, etc. (see Ref. 26). Note that for the doped Mott-insulator we find that the pseudogap is remarkably more pronounced for the SDW-like fluctuations than for CDW-like fluctuations.

There are, however, obvious differences of the case with $U=4t$. For example, the width of the pseudogap appears to be much smaller than 2Δ, being of the order of $\Delta/2$ instead (see Fig. 3). This effect we attribute to the fact that the quasiparticle peak itself is actually strongly narrowed now by the local correlations.

C. Generalized DMFT+$\Sigma_{\mathbf{k}}$ approach: spectral functions $A(\omega,\mathbf{k})$

In the previous subsections we discussed the densities of states obtained self-consistently by the DMFT+$\Sigma_{\mathbf{k}}$ approach. Once we get a self-consistent solution of the DMFT+$\Sigma_{\mathbf{k}}$ equations with nonlocal fluctuations we can, of course, also compute the spectral functions $A(\omega,\mathbf{k})$

$$A(\omega,\mathbf{k}) = -\frac{1}{\pi} \, \text{Im} \, \frac{1}{\omega + \mu - \varepsilon(\mathbf{k}) - \Sigma(\omega) - \Sigma_{\mathbf{k}}(\omega)}, \quad (15)$$

where the self-energy $\Sigma(\omega)$ and the chemical potential μ are calculated self-consistently as described in Sec. II. To plot $A(\omega,\mathbf{k})$ we choose $\mathbf{k}$ points along the bare Fermi surfaces for different types of lattice spectra and filling $n=0.8$. In Fig. 4 one can see corresponding shapes of these bare Fermi surfaces (presented are only $\frac{1}{8}$th of the Fermi surfaces within the first quadrant of the first Brillouin zone).

A natural quantity to inspect is the self-energy $\Sigma(\mathbf{k},\omega+i\delta)$, shown in Fig. 5 for $t'/t=-0.4$, $n=0.8$, and $U=4t$ (left column) and $U=40t$ (right column). As a representative $\mathbf{k}$ points we chose the center of the first Brillouin zone (Γ), the hot-spot and cold-spot (point B in Fig. 4). The results were obtained with NRG at a temperature $T=0.088t$. The structures for $U=4t$ are rather broad, but reveal after a closer inspection features similar to the case $U=40t$. For the latter, the behavior at Γ and B is very different from the structures at the hot-spot. Namely, while for the former two $\mathbf{k}$ points $\text{Im} \, \Sigma(\mathbf{k},\omega+i\delta)$ shows a nice parabolic maximum at the Fermi energy, the latter develops a minimum instead. Such a
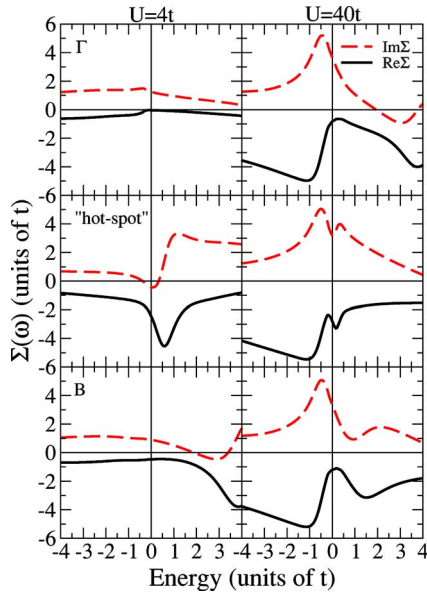
FIG. 5. (Color online) Real (dashed line) and imaginary (full line) parts of the self-energy $\Sigma(\mathbf{k}, \omega)$ for $t/t' = -0.4$, $U = 4t$ (left column), and $U = 40t$ (right column) for characteristic $\mathbf{k}$ points: Γ, hot-spot (see Fig. 4) and cold-spot (point B in Fig. 4). For all graphs the filling is $n = 0.8$, temperature $T = 0.088t$, inverse correlation length $\xi^{-1} = 0.1$, value of pseudogap potential $\Delta = 2t$, and SF combinatorics.

structure in the self-energy will result in a rather evident (pseudo) gap in the spectral function at this $\mathbf{k}$ point and at weaker pseudogap behavior in the DOS. Its appearance is obviously due to the presence of the spin-fluctuations at the hot-spot. Note that similar features have been observed in numerically expensive cluster mean-field calculations,[27] too, with an interpretation as a spin fluctuation induced based on physical expectations. Our calculations, obtained at a minimum numerical expense, indeed show, that including short-ranged fluctuations will precisely produce these non-Fermi-liquid structures in the one-particle self-energy. This behavior is quite typical for the problem and was observed by other groups using different methods.[16,28–30] In several works the midgap peak in the pseudogap was obtained with an explanation of its origin by a particular shape of the self-energy close to the Fermi level.[28,29,31]

In the following we concentrate mainly on the case $U = 4t$ and filling $n = 0.8$ [Fermi surface of Fig. 4(a)]. The corresponding spectral functions $A(\omega, \mathbf{k})$ are depicted in Fig. 6. When $t'/t = -0.4$ (upper row), the spectral function close to the diagonal of the Brillouin zone (point B) has the typical Fermi-liquid behavior, consisting of a rather sharp peak close to the Fermi level. In the case of the SDW-like fluctuations this peak is shifted down in energy by about $-0.5t$ (left upper corner). In the vicinity of the hot-spot the shape of $A(\omega, \mathbf{k})$ is completely modified. Now $A(\omega, \mathbf{k})$ becomes double-peaked and non-Fermi-liquidlike. Directly at the hot-spot, $A(\omega, \mathbf{k})$ for SDW-like fluctuations has two equally intensive peaks situated symmetrically around the Fermi level and split from each other by $\sim 1.5\Delta$ Refs. 4 and 5. For the commensurate CDW-like fluctuations the spectral function in the hot-spot
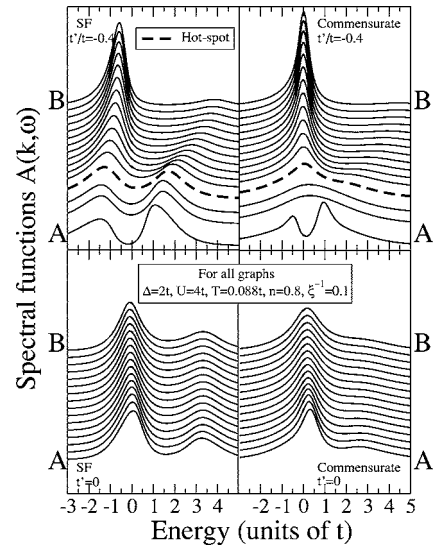

FIG. 6. Spectral functions $A(\mathbf{k}, \omega)$ obtained from the DMFT(NRG)+$\Sigma_{\mathbf{k}}$ calculations along the directions shown in Fig. 4. Model parameters were chosen as $U = 4t$, $n = 0.8$, $\Delta = 2t$, $\xi^{-1} = 0.1$, and temperature $T = 0.088t$. The hot-spot $\mathbf{k}$ point is marked as a fat dashed line. The Fermi level corresponds to zero.

region has one broad peak centered at the Fermi level with the width $\sim \Delta$. Such a merging of the two peaks at the hot spot for commensurate fluctuations was previously observed in Ref. 5. However, close to point $\mathbf{A}$ this type of fluctuations also produces a double-peak structure in the spectral function.

Spectral functions for the case of $U = 4t$ at half-filling ($n = 1$) and for $t'/t = -0.4$ are similar to those just discussed for $n = 0.8$. However, the pseudogap is more pronounced in this case and remains open everywhere close to the Umklapp surface for SDW fluctuations.[26]

In the lower panel of Fig. 6 we show spectral functions for 20% hole doping ($n = 0.8$) and the case of $t' = 0$ [Fermi surface from Fig. 4(b)]. Since the Fermi surface now is close to the Umklapp surface, the pseudogap anomalies are rather strong and almost nondispersive along the Fermi surface. At half filling for $t' = 0$ the Fermi surface actually coincides with the Umklapp surface (in case of perfect nesting the whole Fermi surface is the hot region). The spectral functions are now symmetric around the Fermi level. For SDW-like fluctuations there are two peaks split by $\sim 1.5\Delta$. Again, CDW-like fluctuations give just one peak centered at the Fermi level with width $\sim \Delta$.

For the case of a doped Mott insulator ($U = 40t$, $n = 0.8$), the spectral functions obtained by the DMFT+$\Sigma_{\mathbf{k}}$ approach are presented in Fig. 7. Qualitatively, the shapes of these spectral functions are similar to those shown in Fig. 6. As was pointed out above, the strong Coulomb correlations lead to a narrowing of the quasiparticle peak and a corresponding decrease of the pseudogap width. As is evident from Fig. 7 the structures connected to the pseudogap are now spread in an energy interval $\sim t$, while for $U = 4t$ they are restricted to an interval $\sim 4t$ instead. One should also note that in contrast to $U = 4t$ the spectral functions are now about four times less intensive, because part of the spectral weight is transferred to
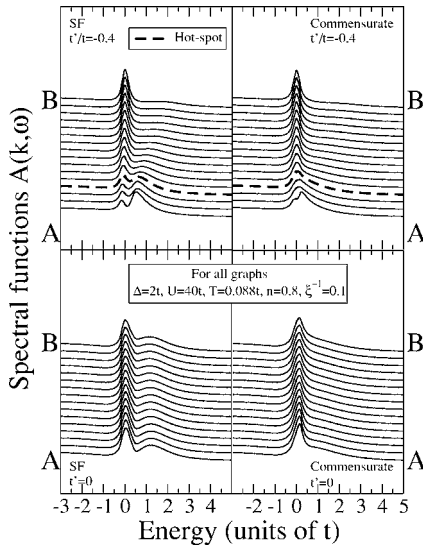
FIG. 7. Spectral functions $A(\mathbf{k}, \omega)$ obtained from the DMFT(NRG)+$\Sigma_{\mathbf{k}}$ calculations for $U=40t$; other parameters as in Fig. 6.

the upper Hubbard band located at about $40t$ and is well separated from the quasiparticle peak now.

Using another quite common choice of $\mathbf{k}$ points we can compute $A(\omega, \mathbf{k})$ along high-symmetry directions in the first Brillouin zone: $\Gamma(0,0)-X(\pi,0)-M(\pi,\pi)-\Gamma(0,0)$. The spectral functions for these $\mathbf{k}$ points are collected in Fig. 8 for the case of SDW-like fluctuations. Characteristic curves for the doped Mott insulator are presented in Ref. 26. For all sets of parameters, one can see a characteristic double-peak pseudogap structure close to the X point. In the middle of the $M-\Gamma$ direction (so called "nodal" point) one can see the reminiscence of the AFM gap which has its biggest value
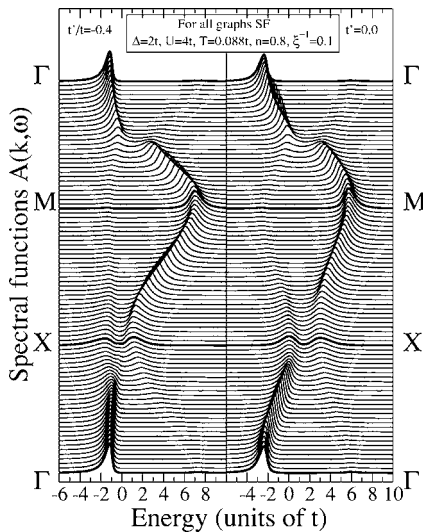

FIG. 8. Spectral functions $A(\mathbf{k}, \omega)$ obtained from the DMFT(NRG)+$\Sigma_{\mathbf{k}}$ calculations along high-symmetry directions of the first Brillouin zone $\Gamma(0,0)-X(\pi,0)-M(\pi,\pi)-\Gamma(0,0)$, *SF* combinatorics (left row) and commensurate combinatorics (right column). Other parameters are $U=4t$, $n=0.8$, $\Delta=2t$, $\xi^{-1}=0.1$, and temperature $T=0.088t$. The Fermi level corresponds to zero.
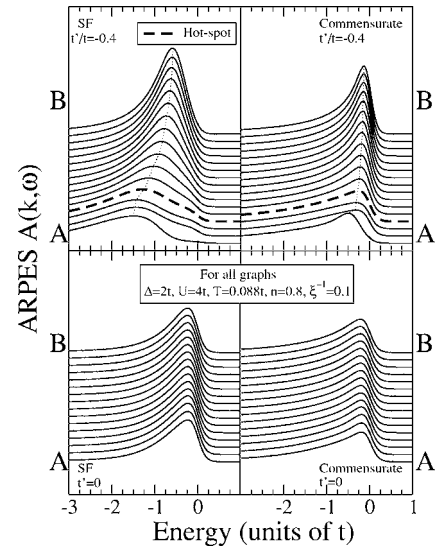
FIG. 9. ARPES spectra simulated by the multiplication of the spectral functions obtained from DMFT(NRG)+$\Sigma_{\mathbf{k}}$ calculations for $U=4t$ and $n=0.8$ in Fig. 6 with the Fermi function at $T=0.088t$ plotted along the lines in the first BZ as depicted by Fig. 4. All other parameters are the same as in Fig. 6.

here in the case of perfect antiferromagnetic ordering. Also in the nodal point "kinklike" behavior is observed caused by interactions between correlated electrons with short-range pseudogap fluctuations. A change of the filling leads mainly to a rigid shift of spectral functions with respect to the Fermi level.

With the spectral functions we are now, of course, in a position to calculate the angle resolved photoemission spectra (ARPES), which is the most direct experimental way to observe pseudogap in real compounds. For that purpose, we only need to multiply our results for the spectral functions with the Fermi function at temperature $T=0.088t$. A typical example of the resulting DMFT+$\Sigma_{\mathbf{k}}$ ARPES spectra are presented in Fig. 9. More figures of ARPES-like results obtained within the DMFT+$\Sigma_{\mathbf{k}}$ approach for a variety of parameters can be found in Ref. 26. One should note that for $t'/t=-0.4$ (upper panel of Fig. 9) as $\mathbf{k}$ goes from point A to point B the peak situated slightly below the Fermi level changes its position and moves down in energy. Simultaneously it becomes more broad and less intensive. The dotted line guides the motion of the peak maximum. Also at the hot spot and further to point B one can see some signs of the double-peak structure. Such behavior of the peak in the ARPES is rather reminiscent of those observed experimentally in underdoped cuprates.[2,4,32]

V. CONCLUSION

In summary, we propose a generalized DMFT+$\Sigma_{\mathbf{k}}$ approach, which is meant to take into account the important effects of nonlocal correlations (in principle of any type) in addition to the (essentially exact) treatment of local dynamical correaltions by the DMFT. In the standard DMFT the "bath" surrounding the effective single Anderson impurity is

spatially uniform since the DMFT self-energy is only energy dependent. The main idea of our extension is to introduce nonlocal correlations through the bath, i.e. to make it spatially nonuniform, while keeping standard DMFT self-consistency equations. Such a generalization of the DMFT allows us to supplement it with a **k**-dependent self-energy $\Sigma(\mathbf{k}, \omega)$. It in turn opens the possibility of accessing the physics of low-dimensional strongly correlated systems, where different types of spatial fluctuations (e.g., of some order parameter) become important, in a nonperturbative way at least with respect to the important local dynamical correlations. However, we must stress that our procedure in no way introduces any kind of systematic $1/d$ expansion, being only a qualitative method to include a length scale into the DMFT. Nevertheless, we believe that such a technique can give valuable insight into the physical processes leading to the correlation induced **k**-dependent structures in single-particle properties.

In this work we model such effects for the two-dimensional Hubbard model by incorporating into the bath scattering of fermions from nonlocal collective SDW-like antiferromagnetic spin (or CDW-like charge) short-range fluctuations. The corresponding **k**-dependent self-energy $\Sigma(\mathbf{k}, \omega)$ is obtained from a nonperturbative iterative scheme.[4,5] Such a choice of the $\Sigma(\mathbf{k}, \omega)$ allows us to address the problem of pseudogap formation in the strongly correlated metallic state. We showed evidence that the pseudogap appears at the Fermi level within the quasiparticle peak, introducing a new small energy scale of the order of pseudogap potential value Δ in the DOS and more pronounced in spectral functions $A(\omega, \mathbf{k})$. Let us stress that our generalization of the DMFT leads to nontrivial and in our opinion physically sensible **k** dependence of spectral functions. It is significant that this particular choice of $\Sigma(\mathbf{k}, \omega)$ (Refs. 4 and 5) does not cause difficulties to "double counting" problems within our combined DMFT+$\Sigma_\mathbf{k}$ approach. Also, the combination of diagrammatically correct techniques such as DMFT (Refs. 6–10) and the nonlocal self-energy ansatz of Refs. 4 and 5 preserves the correct analytical properties of the combined self-energy $\Sigma(i\omega) + \Sigma_\mathbf{k}(i\omega)$, as well as of the corresponding one-electron propagator (1).

Of course, our pseudogap observations are not entirely new. Similar results about pseudogap formation in the $2d$ Hubbard model were already obtained within cluster DMFT extensions, i.e., the dynamical cluster approximation (DCA) (Refs. 12 and 27) and the cellular DMFT (CDMFT),[16,17] CPT,[14,15,33] and two interacting Hubbard sites self-consistently embedded in a bath.[28] However, these methods have generic restrictions concerning the size of the cluster, temperature, or filling accessible and, in the case of the QMC, values of the local Coulomb energy. Recently, the EDMFT was also applied to demonstrate the pseudogap formation in the DOS due to dynamic Coulomb correlations.[34] Note, however, that within the EDMFT there is no way to obtain a **k** dependence in spectral functions beyond that originating from the bare electronic energy dispersion. Important progress was also made with the weak coupling approaches for the Hubbard model[35] and the functional renormalization group.[29,30] In several papers, pseudogap

formation was described in the framework of the t-J model.[36] A more general scheme for the inclusion of nonlocal corrections was also formulated within the so called GW extension to the DMFT.[37,38]

While at a first glance the introduction of additional phenomenological parameters (correlation length ξ and pseudogap strength Δ) through the definition of $\Sigma(\mathbf{k}, \omega)$ seems to take a step back with respect to the methods outlined above, it actually opens up the possibility to systematically distinguish between different types of nonlocal fluctuations and their effects and help to analyze experimental or theoretical data obtained within more advanced schemes in terms of intuitive physical pictures. Note, however, that in principle even the parameters ξ and Δ can be calculated from the original model.[23]

An essential advantage of the proposed combination of two nonperturbative methods [DMFT and $\Sigma(\mathbf{k}, \omega)$ from Refs. 4 and 5] removes the restrictions on model parameters in, e.g., cluster mean-field theories. Our scheme works for any Coulomb interaction strength U, pseudogap strength Δ, correlation length ξ, filling n, and bare electron dispersion $\varepsilon(\mathbf{k})$ on a $2d$ square lattice for any set of **k** points. Although we presented only high-temperature data in this paper, the possibility of using Wilson's NRG to solve the effective impurity model also opens the possibiltiy of studying properties at $T = 0$, which is currently impossible within the DCA or CDMFT for larger clusters. Moreover, the DMFT+$\Sigma_\mathbf{k}$ approach can be easily generalized to orbital degrees of freedom, phonons, impurities, etc.

As a further application of our generalized DMFT+$\Sigma_\mathbf{k}$ we would like to bring the reader's attention to Ref. 39, which deals with the problem of the Fermi surface destruction in high-T_c compounds because of pseudogap fluctuations.

APPENDIX A: DERIVATION OF GENERALIZED DMFT+$\Sigma_\mathbf{k}$ APPROACH

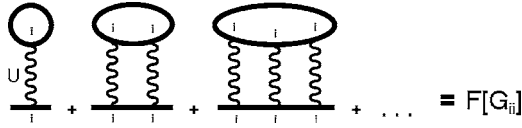In this Appendix we present a derivation of the generalized DMFT+$\Sigma_\mathbf{k}$ scheme for the Hubbard model

FIG. 10. Local skeleton diagrams for the DMFT self-energy Σ. Wavy lines represent the local (Hubbard) Coulomb interaction U; full lines denote the local Green function G_{ii}.

$$H = -\sum_{ij,\sigma} t_{ij} c_{i\sigma}^{\dagger} c_{j\sigma} + U \sum_{i} n_{i\uparrow} n_{i\downarrow}, \quad (A1)$$

using a diagrammatic approach. The single-particle Green function in Matsubara representation is as usual given by

$$G_{\mathbf{k}}(i\omega) = \frac{1}{i\omega + \mu - \varepsilon(\mathbf{k}) - \Sigma(i\omega, \mathbf{k})}. \quad (A2)$$

To establish the standard DMFT one invokes the limit of infinite dimensions $d \to \infty$. In this limit only local contributions to the electron self-energy survive,[7,9] i.e., $\Sigma_{ij} \to \delta_{ij} \Sigma_{ii}$ or, in reciprocal space, $\Sigma(i\omega, \mathbf{k}) \to \Sigma(i\omega)$.

In Fig. 10 we show examples of skeleton diagrams for the local self-energy, contributing in the limit of $d \to \infty$. The complete series of these and similar diagrams defines the local self-energy as a functional of the local Green function

$$\Sigma = F[G_{ii}], \quad (A3)$$

where

$$G_{ii}(i\omega) = \frac{1}{N} \sum_{\mathbf{k}} \frac{1}{i\omega + \mu - \varepsilon(\mathbf{k}) - \Sigma(i\omega)}. \quad (A4)$$

One then defines the Weiss field

$$\mathcal{G}_0^{-1}(i\omega) = \Sigma(i\omega) + G_{ii}^{-1}(i\omega) \quad (A5)$$

which is used to set up the effective single impurity problem with an effective action given by (5). In Dyson's equation, the Green function (4) for this effective single impurity problem can be written as

$$G_d(i\omega) = \frac{1}{\mathcal{G}_0^{-1}(i\omega) - \Sigma_d(i\omega)}, \quad (A6)$$

and the skeleton diagrams for self-energy Σ_d are just the same as shown in Fig. 10, with the replacement $G_{ii} \to G_d$. Thus we get

$$\Sigma_d = F[G_d], \quad (A7)$$

where F is the same functional as in (A3). The two equations (A6) and (A7) define both G_d and Σ_d for a given Weiss field $\mathcal{G}_0$. On the other hand, for the local Σ and G_{ii} of the initial (Hubbard) problem we have precisely the same pair of equations, (A3) and (A5), and $\mathcal{G}_0$ in both problems is just the same, so that

$$\Sigma = \Sigma_d; \quad G_{ii} = G_d. \quad (A8)$$

Thus, the task of finding the local self-energy of the $(d \to \infty)$ Hubbard model is eventually reduced to the calculation of the self-energy of an effective quantum single impu-
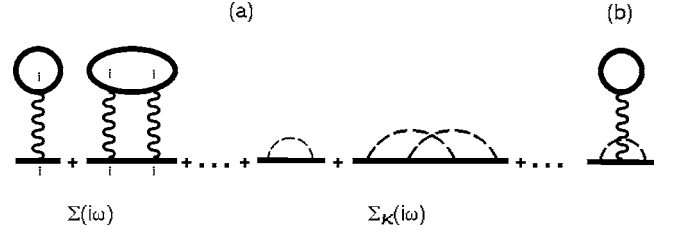

FIG. 11. Typical skeleton diagrams for the self-energy in the DMFT$+\Sigma_{\mathbf{k}}$ approach. The first two terms are DMFT self-energy diagrams; the middle two diagrams show contributions to the non-local part of the self-energy from spin fluctuations (see Sec. III) represented as dashed lines; the last diagram (b) is an example of the neglected diagram leading to the interference between the local and nonlocal parts.

rity problem defined by the effective action of Eq. (5).

Consider now the nonlocal contribution to the self-energy. If we neglect interference between local and nonlocal contributions [as given, e.g., by the diagram shown in Fig. 11(b)], the full self-energy is approximately determined by the sum of these two contributions. Skeleton diagrams for the nonlocal part of the self-energy, $\Sigma_{\mathbf{k}}(i\omega)$, are then those shown in Fig. 11(a), where the full line denotes the Green function $G_{\mathbf{k}}$ of Eq. (1), while dashed lines denote the interaction with static Gaussian spin (charge) fluctuations. These diagrams are just absent within the standard DMFT (as any contribution from Ornstein–Zernike type fluctuations vanish for $d \to \infty$), and no double counting problems arise at all.

The local contribution to the self-energy is again defined by the functional (A3) via the local Green function G_{ii}, which is now given by Eq. (2). Introducing again a Weiss field via (A5) and repeating all previous arguments, we again reduce the task of finding the local part of the self-energy to the solution of a single impurity problem with an effective action (5).

To determine the nonlocal contribution $\Sigma_{\mathbf{k}}(i\omega)$ we first introduce

$$\mathcal{G}_{0\mathbf{k}}(i\omega) = \frac{1}{G_{\mathbf{k}}^{-1}(i\omega) + \Sigma_{\mathbf{k}}(i\omega)} = \frac{1}{i\omega + \mu - \varepsilon(\mathbf{k}) - \Sigma(i\omega)} \quad (A9)$$

as the bare Green function for electron scattering by static Gaussian spin (charge) fluctuations. The assumed static nature of these fluctuations allows one to use the method of Refs. 4, 5, and 22 and the calculation of the nonlocal part of the self-energy $\Sigma_{\mathbf{k}}(i\omega)$ reduces to the recursion procedure defined by Eqs. (8) and (9). The choice of the bare Green function Eq. (A9) guarantees that the Green function dressed by fluctuations $G_{\mathbf{k}}^{-1}(i\omega) = \mathcal{G}_{0\mathbf{k}}^{-1}(i\omega) - \Sigma_{\mathbf{k}}(i\omega)$, which enters into the skeleton diagrams for $\Sigma_{\mathbf{k}}(i\omega)$, just coincides with the full Green functions $G_{\mathbf{k}}(i\omega)$.

Thus we obtain a fully self-consistent scheme to calculate both local (due to strong single-site correlations) and nonlocal (due to short-range fluctuations) contributions to electron self-energy.

APPENDIX B: Δ IN THE HUBBARD MODEL

In this Appendix we derive the explicit microscopic expression for pseudogap amplitude Δ given in Eq. (13).

Within the two-particle self-consistent approach of Ref. 23, valid for medium values of U, and neglecting charge fluctuations, we can write down an expression for the electron self-energy of the form used in Eq. (1), with

$$\Sigma_\sigma(i\omega) = U n_{-\sigma} \qquad (B1)$$

as the lowest order local contribution due to the on-site Hubbard interaction, surviving in the limit of $d \to \infty$, and exactly accounted for in the DMFT (with all higher-order contributions). Nonlocal contribution to the self-energy (vanishing for $d \to \infty$ and not accounted within the DMFT) due to interaction with spin-fluctuations then leads to the expression

$$\Sigma_{\mathbf{k}}(i\omega) = \frac{U}{4} \frac{T}{N} \sum_m \sum_{\mathbf{q}} U_{sp} \chi_{sp}(\mathbf{q}, \nu_m) G_0(\mathbf{k} + \mathbf{q}, i\omega + i\nu_m),$$

$$(B2)$$

where

$$U_{sp} = g_{\uparrow\downarrow}(0) U, \quad g_{\uparrow\downarrow}(0) = \frac{\langle n_{i\uparrow} n_{i\downarrow}\rangle}{\langle n_{i\uparrow}\rangle\langle n_{i\downarrow}\rangle} \qquad (B3)$$

with $\langle n_\sigma^2 \rangle = \langle n_\sigma \rangle$ and $\langle n_{i\uparrow} \rangle = \langle n_{i\downarrow} \rangle = \frac{1}{2} n$ in the paramagnetic phase. For the dynamic spin susceptibility $\chi_{sp}(\mathbf{q}, \nu_m)$ we use the standard Ornstein–Zernike form,[23] similar to that used in the spin-fermion model,[4] which describes the enhanced scattering with momenta transfer close to the antiferromagnetic vector $\mathbf{Q} = (\pi/a, \pi/a)$. With these approximations, we can write down the following expression for the nonlocal contribution to the self-energy:[4,5]

$$\Sigma_{\mathbf{k}}(i\omega) = \frac{1}{4} U U_{sp} \frac{T}{N} \sum_m \sum_{\mathbf{q}} \chi_{sp}(\mathbf{q}, \nu_m) \frac{1}{i\omega + i\nu_m + \mu - \varepsilon(\mathbf{k} + \mathbf{q})} \approx \frac{1}{4} U U_{sp} \frac{T}{N} \sum_m \sum_{\mathbf{q}} \chi_{sp}(\mathbf{q}, \nu_m) \sum_{\mathbf{q}} S(\mathbf{q}) \frac{1}{i\omega + \mu - \varepsilon(\mathbf{k} + \mathbf{q})}$$

$$\equiv \Delta^2 \sum_{\mathbf{q}} S(\mathbf{q}) \frac{1}{i\omega + \mu - \varepsilon(\mathbf{k} + \mathbf{q})} = \frac{\Delta^2}{i\omega + \mu - \varepsilon(\mathbf{p} + \mathbf{Q}) + i(|v_{\mathbf{p}+\mathbf{Q}}^x| + |v_{\mathbf{p}+\mathbf{Q}}^y|)\kappa \, \text{sign} \, \omega}. \qquad (B4)$$

Here we have introduced the static form factor (Ref. 5)

$$S(\mathbf{q}) = \frac{2\xi^{-1}}{(q_x - Q_x)^2 + \xi^{-2}} \frac{2\xi^{-1}}{(q_y - Q_y)^2 + \xi^{-2}} \qquad (B5)$$

and the squared pseudogap amplitude

$$\Delta^2 = \frac{1}{4} U U_{sp} \frac{T}{N} \sum_m \sum_{\mathbf{q}} \chi_{sp}(\mathbf{q}, \nu_m)$$

$$= \frac{1}{4} U U_{sp} [\langle n_{i\uparrow} \rangle + \langle n_{i\downarrow} \rangle - 2\langle n_{i\uparrow} n_{i\downarrow} \rangle] = \frac{1}{4} U U_{sp} \frac{1}{3} \langle \vec{S}_i^2 \rangle,$$

$$(B6)$$

where we have used the exact sum rule for the susceptibility.[4,23] Taking into account Eq. (B3) we immediately obtain Eq. (13).

Actually, the approximations made in Eqs. (B4) and (B5) allow for an exact summation of the whole Feynman series for the electron interaction with spin fluctuations, replaced by the static Gaussian random field. Thus generalizing the one-loop approximation (B4) eventually leads to the basic recursion procedure given in Eqs. (9) and (8) and Refs. 4 and 5.

Using the DMFT(QMC) approach we computed occupancies $\langle n_{i\uparrow} \rangle$, $\langle n_{i\downarrow} \rangle$ and double occupancies $\langle n_{i\uparrow} n_{i\downarrow} \rangle$ required to calculate the pseudogap amplitude Δ of Eq. (B6). In Fig. 12 the corresponding values of Δ are presented. One can see that Δ grows when the filling goes to $n=1$. While U approaches $8t$ (the value of the bandwidth for a square lattice)

Δ as a function of n grows monotonically. When U becomes larger than $W=8t$ (when a metal-insulator transition occurs) one can see a local minimum for $n=0.9$, which becomes more pronounced with further increase of U. For $t'/t=-0.4$ and both temperatures, the scatter of Δ values is smaller than for the case of $t'=0$. Also Δ has a rather weak temperature dependence. All values of Δ lie in the interval $\sim 0.75t \div 2t$. Therefore, for our computations we took only two characteristic values of $\Delta = t$ and $\Delta = 2t$.
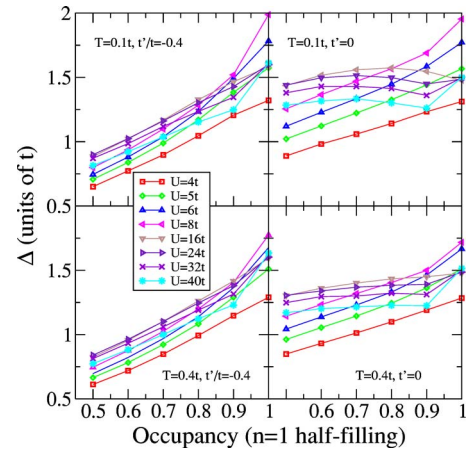

FIG. 12. (Color online) Filling dependence of the pseudogap potential Δ calculated with the DMFT(QMC) for the varying Coulomb interaction (U) and the temperature (T) on a two-dimensional square lattice with two sets of (t, t').

[1] T. Timusk and B. Statt, Rep. Prog. Phys. **62**, 61 (1999).

[2] M. V. Sadovskii, Usp. Fiz. Nauk **171**, 539 (2001) [Phys. Usp. **44**, 515 (2001)].

[3] D. Pines, ArXiv: cond-mat/0404151 (unpublished).

[4] J. Schmalian, D. Pines, and B. Stojkovic, Phys. Rev. Lett. **80**, 3839 (1998); Phys. Rev. B **60**, 667 (1999).

[5] E. Z. Kuchinskii and M. V. Sadovskii, Zh. Eksp. Teor. Fiz. **115**, 1765 (1999) [JETP **88**, 347 (1999)] [available as ArXiv: cond-mat/9808321 (unpublished)].

[6] W. Metzner and D. Vollhardt, Phys. Rev. Lett. **62**, 324 (1989).

[7] D. Vollhardt, in *Correlated Electron Systems*, edited by V. J. Emery (World Scientific, Singapore, 1993), p. 57.

[8] Th. Pruschke, M. Jarrell, and J. K. Freericks, Adv. Phys. **44**, 187 (1995).

[9] A. Georges, G. Kotliar, W. Krauth, and M. J. Rozenberg, Rev. Mod. Phys. **68**, 13 (1996).

[10] G. Kotliar and D. Vollhardt, Phys. Today **57**(3), 53 (2004).

[11] Q. Si and J. L. Smith, Phys. Rev. Lett. **77**, 3391 (1996).

[12] Th. Maier, M. Jarrell, Th. Pruschke, and M. Hettler, Rev. Mod. Phys. [in print, ArXiv: cond-mat/0404055 (unpublished)].

[13] G. Kotliar, S. Y. Savrasov, G. Palsson, and G. Biroli, Phys. Rev. Lett. **87**, 186401 (2001); for periodized version (PCDMFT), see M. Capone, M. Civelli, S. S. Kancharla, C. Castellani, and G. Kotliar, Phys. Rev. B **69**, 195105 (2004).

[14] C. Gros and R. Valenti, Ann. Phys. **3**, 460 (1994).

[15] D. Senechal, D. Perez, and M. Pioro-Ladriee, Phys. Rev. Lett. **84**, 522 (2000); D. Senechal, D. Perez, and D. Plouffe, Phys. Rev. B **66**, 075129 (2002).

[16] B. Kyung, S. S. Kancharla, D. Senechal, A.-M. S. Tremblay, M. Civelli, and G. Kotliar, ArXiv: cond-mat/0502565 (unpublished).

[17] M. Civelli, M. Capone, S. S. Kancharla, O. Parcollet, and G. Kotliar, Phys. Rev. Lett. **95**, 106402 (2005).

[18] J. E. Hirsch and R. M. Fye, Phys. Rev. Lett. **56**, 2521 (1986); M. Jarrell, Phys. Rev. Lett. **69**, 168 (1992); M. J. Rozenberg, X. Y. Zhang, and G. Kotliar, *ibid.* **69**, 1236 (1992); A. Georges and W. Krauth, *ibid.* **69**, 1240 (1992); M. Jarrell, in *Numerical Methods for Lattice Quantum Many-Body Problems*, edited by D. Scalapino (Addison Wesley, 1997). For a review of QMC for DMFT see Ref. 19.

[19] K. Held, I. A. Nekrasov, N. Blümer, V. I. Anisimov, and D. Vollhardt, Int. J. Mod. Phys. B **15**, 2611 (2001); K. Held, I. A. Nekrasov, G. Keller, V. Eyert, N. Blümer, A. K. McMahan, R. T. Scalettar, T. Pruschke, V. I. Anisimov, and D. Vollhardt, ArXiv: cond-mat/0112079 published in *Quantum Simulations of Complex Many-Body Systems: From Theory to Algorithms*, edited by J. Grotendorst, D. Marks, and A. Muramatsu, NIC Series Volume 10 (NIC Directors, Forschunszentrum Jülich, 2002) pp. 175–209.

[20] K. G. Wilson, Rev. Mod. Phys. **47**, 773 (1975); H. R. Krishnamurthy, J. W. Wilkins, and K. G. Wilson, Phys. Rev. B **21**, 1003 (1980); **21**, 1044 (1980); for a comprehensive introduction to NRG, see e.g., A. C. Hewson, in *The Kondo Problem to Heavy Fermions* (Cambridge University Press, Cambridge, 1993).

[21] R. Bulla, A. C. Hewson, and Th. Pruschke, J. Phys.: Condens. Matter **10**, 8365 (1998); R. Bulla, Phys. Rev. Lett. **83**, 136 (1999).

[22] M. V. Sadovskii, Zh. Eksp. Teor. Fiz. **77**, 2070 (1979) [Sov. Phys. JETP **50**, 989 (1979)].

[23] Y. M. Vilk and A.-M. S. Tremblay, J. Phys. I **7**, 1309 (1997).

[24] O. Gunnarsson, O. K. Andersen, O. Jepsen, and J. Zaanen, Phys. Rev. B **39**, 1708 (1989).

[25] M. T. Czyzyk and G. A. Sawatzky, Phys. Rev. B **49**, 14211 (1994).

[26] M. V. Sadovskii, I. A. Nekrasov, E. Z. Kuchinskii, Th. Prushke, and V. I. Anisimov, ArXiv: cond-mat/0502612 (unpublished).

[27] Th. A. Maier, Th. Pruschke, and M. Jarrell, Phys. Rev. B **66**, 075102 (2002).

[28] T. D. Stanescu and P. Phillips, Phys. Rev. Lett. **91**, 017002 (2003).

[29] A. A. Katanin and A. P. Kampf, Phys. Rev. Lett. **93**, 106406 (2004).

[30] D. Rohe and W. Metzner, Phys. Rev. B **71**, 115116 (2005).

[31] D. K. Sunko and S. Barisic, Eur. Phys. J. B **46**, 269 (2005).

[32] A. Kaminski, H. M. Fretwell, M. R. Norman, M. Randeria, S. Rosenkranz, U. Chatterjee, J. C. Campuzano, J. Mesot, T. Sato, T. Takahashi, T. Terashima, M. Takano, K. Kadowaki, Z. Z. Li, and H. Raffy, Phys. Rev. B **71**, 014517 (2005).

[33] D. Senechal and A.-M. S. Tremblay, Phys. Rev. Lett. **92**, 126401 (2004).

[34] K. Haule, A. Rosch, J. Kroha, and P. Wölfle, Phys. Rev. Lett. **89**, 236402 (2002); Phys. Rev. B **68**, 155119 (2003).

[35] B. Kyung, V. Hankevych, A.-M. Dare, and A.-M. S. Tremblay, Phys. Rev. Lett. **93**, 147004 (2004).

[36] P. Prelovsek and A. Ramsak, Phys. Rev. B **63**, 180506(R) (2001); P. Prelovsek and A. Ramsak, *ibid.* **72**, 012510 (2005).

[37] S. Biermann, F. Aryasetiawan, and A. Georges, Phys. Rev. Lett. **90**, 086402 (2003).

[38] P. Sun and G. Kotliar, Phys. Rev. Lett. **92**, 196402 (2004).

[39] E. Z. Kuchinskii, I. A. Nekrasov, and M. V. Sadovskii, JETP Lett. **82**, 198 (2005)[Pis'ma Zh. Eksp. Teor. Fiz. **82**, 217 (2005)].

[40] Discretization parameter $\Lambda = 2$, the number of low energy states after the truncation 1000, cut off near Fermi energy 10^{-6}, broadening parameter $b = 0.6$.

[41] Number warm-up sweeps 30000, the number of QMC sweeps 200 000, the number of imaginary time slices 40.

[42] We have checked that with the increase of Coulomb repulsion, the Van–Hove singularity *gradually* transforms into quasiparticle peak for $U = (6 \div 8)t$.